

Photoproduction of $a_2(1320)$ in a Regge modelXiao-Yun Wang^{1,2,3,*} and Alexey Guskov^{4,†}¹*Institute of Modern Physics, Chinese Academy of Sciences, Lanzhou 730000, China*²*University of Chinese Academy of Sciences, Beijing 100049, China*³*Research Center for Hadron and CSR Physics, Institute of Modern Physics of CAS and Lanzhou University, Lanzhou 730000, China*⁴*Joint Institute for Nuclear Research, Dubna 141980, Russia*

(Received 26 November 2015; published 14 April 2016)

In this work, the photoproduction of $a_2(1320)$ off a proton target is investigated within an effective Lagrangian approach and the Regge model. The theoretical result indicates that the shapes of the total and differential cross sections of the $\gamma p \rightarrow a_2^+ n$ reaction within the Feynman (isobar) model are much different from that of the Reggeized treatment. The obtained cross section is compared with the existing experimental results at low energies. The $a_2(1320)$ production cross section at high energies can be tested by the COMPASS experiment, which can provide important information for clarifying the role of the Reggeized treatment at that energy range.

DOI: 10.1103/PhysRevD.93.074016

I. INTRODUCTION

Within the past decades great progress has been achieved in hadron spectroscopy [1,2]. Especially, inspired by the observation of exotic states [1,2] (such as the candidate for the tetraquark [3] or pentaquark [4] state), the underlying structure of these states attracts much attention in both theory and experiment. Observation of the exclusive photoproduction of exotic hadronic states off baryons, proposed in Refs. [5–9], is the most direct way to get information about their nature. At higher energies such processes can be described in terms of Regge trajectory exchanges [10,11]. In Ref. [12], the η and η' photoproduction were studied with the Reggeized model. It is found that the Reggeized model gives a good description for these reactions in and beyond the resonance region. Thus the photoproduction reaction at high energy may be appropriate to study the role of Reggeized treatment.

In the 1950s, Regge proved the importance of extending the angular momentum J to the complex field [13,14]. For more general reviews about the Regge theory, see Refs. [15–17]. Later, the exchange of dominant meson Regge trajectories was used to successfully describe the hadron photoproduction [18–21]. However, there is one question: has the Regge trajectory approach been well tested by experiment at higher energies?

In the past, the $a_2(1320)$ ($\equiv a_2$) photoproduction was extensively studied. The estimation of the exclusive photoproduction cross section for a_2 has been performed according to the one-pion exchange (OPE) mechanism with absorption in [22]. The experimental results for the values and energy dependence of this cross section at relatively

low (<20 GeV) energies are quite consistent with the prediction of this model [23]. Nevertheless the energy range covered by the existing experimental data is not enough to distinguish between the OPE prediction and the Regge trajectory approach [24].

The COMPASS experiment at CERN, which uses the muon beam, can significantly enlarge the available energy range of virtual photons up to about 150 GeV. COMPASS has a good opportunity to contribute to the study of exotic charmonia via their photoproduction. However, the uncertainties of the theoretical description of photon-nucleon interaction at high energies complicate this task. The process of $\gamma^* p \rightarrow a_2^+ n$, where γ^* is a virtual photon, has a quite good experimental signature and can be used as a benchmark. The possibility to use a_2 photoproduction as a benchmark for the study of exotic hadrons is discussed also in [25]. It is also significant to carry out more theoretical studies on the $\gamma p \rightarrow a_2^+ n$ process in order to clarify the role of the Reggeized treatment.

Moreover, because of the vector meson dominance (VMD) assumption, a photon can interact with a vector meson, which means that the $\gamma p \rightarrow a_2^+ n$ reaction can also proceed through the VMD mechanism [26–28]. Thus the a_2 photoproduction mechanism is also an interesting issue.

In this work, the $\gamma p \rightarrow a_2^+ n$ reaction is investigated using an effective Lagrangian approach and the Regge model. In addition to the π exchange, the contributions from the VMD mechanism are also considered. The differential cross section of the $\gamma p \rightarrow a_2^+ n$ reaction is also calculated, which could be tested by further COMPASS experiments.

This paper is organized as follows. After the Introduction, we present the formalism and the main ingredients which are used in our calculation. The numerical results and discussions are given in Sec. III. In Sec. IV,

*xywang@impcas.ac.cn
†avg@jinr.ru

we give a detailed illustration of the possibility of the experimental test at COMPASS. Finally, the paper ends with a brief summary.

II. FORMALISM

In the present work, an effective Lagrangian approach in terms of hadrons is adopted, which is an important theoretical method in investigating various scattering processes [29–34].

Figure 1 describes the basic tree-level Feynman diagrams for the $a_2(1320)$ photoproduction process through general π exchange [Fig. 1(a)] and the VMD mechanism [Fig. 1(b)] [26–28].

To gauge the contribution of this diagram, we need to know the relevant effective Lagrangian densities.

For the πNN interaction vertex we take the effective pseudoscalar coupling [35],

$$\mathcal{L}_{\pi NN} = -ig_{\pi NN} \bar{N} \gamma_5 \vec{\tau} \cdot \vec{\pi} N, \quad (1)$$

where $\vec{\tau}$ is the Pauli matrix, while N and π stand for the fields of the nucleon and the pion, respectively. The coupling constant of the πNN interaction was given in many theoretical works, and we take $g_{\pi NN}^2/4\pi = 12.96$ [36,37].

The commonly employed Lagrangian densities for $a_2\pi\gamma$ and $a_2\pi\rho$ couplings are [38–41]

$$\mathcal{L}_{a_2\pi\gamma} = \frac{g_{a_2\pi\gamma}}{m_\pi^2} \epsilon_{\mu\nu\alpha\beta} \partial^\mu a_2^{\nu\sigma} \partial^\alpha A^\beta \partial_\sigma \phi_\pi, \quad (2)$$

$$\mathcal{L}_{a_2\pi\rho} = \frac{g_{a_2\pi\rho}}{m_\pi^2} \epsilon_{\mu\nu\alpha\beta} \partial^\mu a_2^{\nu\sigma} \partial^\alpha \rho^\beta \partial_\sigma \phi_\pi, \quad (3)$$

where A^β , $a_2^{\nu\sigma}$, ρ^β , and ϕ_π are the photon, a_2 meson, ρ and π fields. m_π is the mass of the π meson. The coupling

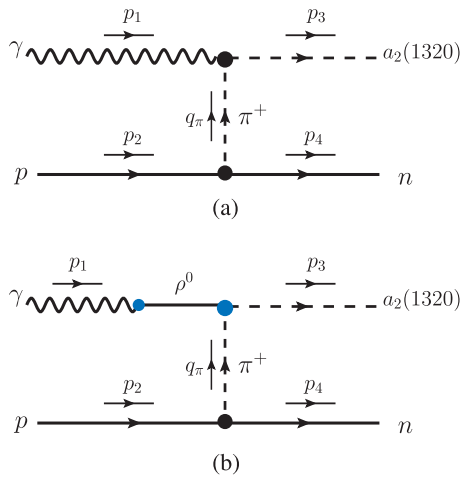


FIG. 1. (a) Feynman diagrams for the $\gamma p \rightarrow a_2 n$ reaction via π exchange. (b) Same as in (a), but for the case in the frame of the VMD model.

constants $g_{a_2\pi\gamma}$ and $g_{a_2\pi\rho}$ can be determined by the partial decay widths $\Gamma_{a_2 \rightarrow \pi\gamma}$ and $\Gamma_{a_2 \rightarrow \pi\rho}$, respectively. With the above Lagrangian densities, we obtain

$$\Gamma_{a_2 \rightarrow \pi\gamma} = \frac{g_{a_2\pi\gamma}^2}{10\pi m_\pi^4} |\vec{p}_\gamma^{\text{c.m.}}|^5, \quad (4)$$

$$\Gamma_{a_2 \rightarrow \pi\rho} = \frac{g_{a_2\pi\rho}^2}{10\pi m_\pi^4} |\vec{p}_\rho^{\text{c.m.}}|^5, \quad (5)$$

with

$$|\vec{p}_\gamma^{\text{c.m.}}| = \frac{\lambda^{1/2}(M_{a_2}^2, m_\pi^2, m_\gamma^2)}{2M_{a_2}}, \quad (6)$$

$$|\vec{p}_\rho^{\text{c.m.}}| = \frac{\lambda^{1/2}(M_{a_2}^2, m_\pi^2, m_\rho^2)}{2M_{a_2}}, \quad (7)$$

where λ is the Källén function with $\lambda(x, y, z) = (x - y - z)^2 - 4yz$. Using the partial decay widths of $a_2(1320)$ as listed in the PDG book [42], we get $g_{a_2\pi\gamma} = 0.539 \times 10^{-2} \text{ GeV}^{-1}$ and $g_{a_2\pi\rho} = 0.268 \text{ GeV}^{-1}$.

For the $a_2\gamma\pi$ interaction vertex we can also derive it using the VMD mechanism [26–28] on the assumption that the coupling is due to a sum of intermediate vector mesons. In the VMD mechanism for photoproduction, a real photon can fluctuate into a virtual vector meson, which subsequently scatters from the target proton. Under the VMD mechanism, the Lagrangian of depicting the coupling of the intermediate vector meson ρ with a photon is written as

$$\mathcal{L}_{\rho\gamma} = -\frac{em_\rho^2}{f_\rho} V_\mu A^\mu, \quad (8)$$

where m_ρ^2 and f_ρ are the mass and the decay constant of the ρ meson, respectively. With the above equation, we get the expression for the $\rho \rightarrow e^+e^-$ decay,

$$\Gamma_{\rho \rightarrow e^+e^-} = \left(\frac{e}{f_\rho}\right)^2 \frac{8\alpha |\vec{p}_e^{\text{c.m.}}|^3}{3m_\rho^2}, \quad (9)$$

where $\vec{p}_e^{\text{c.m.}}$ indicates the three-momentum of an electron in the rest frame of the ρ meson, while $\alpha = e^2/4\hbar c = 1/137$ is the electromagnetic fine structure constant. Thus, with the partial decay width of $\rho \rightarrow e^+e^-$ [42]

$$\Gamma_{\rho \rightarrow e^+e^-} = 7.04 \text{ keV}, \quad (10)$$

we get the constant $e/f_\rho \approx 0.06$.

To account for the internal structure of hadrons, we introduce phenomenological form factors. For the vertex of $a_2\pi\rho$, the following form factor is adopted [31,43,44]:

$$\mathcal{F}_{a_2\pi\rho}(q_\pi^2) = \frac{m_\rho^2 - m_\pi^2}{m_\rho^2 - q_\pi^2}. \quad (11)$$

For the vertices of πNN and $a_2\pi\gamma$, three types of the form factors are considered [31,43–46]: (i) the monopole form factor

$$\mathcal{F}_{\pi NN}(q_\pi^2) = \mathcal{F}_{a_2\pi\gamma}(q_\pi^2) = \frac{\Lambda_t^2 - m_\pi^2}{\Lambda_t^2 - q_\pi^2}, \quad (12)$$

(ii) the dipole form factor

$$\mathcal{F}_{\pi NN}(q_\pi^2) = \mathcal{F}_{a_2\pi\gamma}(q_\pi^2) = \left(\frac{\Lambda_d^2 - m_\pi^2}{\Lambda_d^2 - q_\pi^2} \right)^2, \quad (13)$$

(iii) the exponential form factor

$$\mathcal{F}_{\pi NN}(q_\pi^2) = \mathcal{F}_{a_2\pi\gamma}(q_\pi^2) = \exp \left[R^2 \frac{(t - m_\pi^2)}{(1 - X_L)} \right], \quad (14)$$

where Λ_t , Λ_d , and R are the free parameters, which can be determined from the data in this work. X_L is the momentum fraction of the proton carried by the neutron.

With the effective Lagrangian densities as listed above, the invariant scattering amplitudes for the $\gamma(p_1)p(p_2) \rightarrow a_2^+(p_3)n(p_4)$ process can be written as

$$\begin{aligned} \mathcal{M}_a &= \sqrt{2} \frac{g_{\pi NN} g_{a_2\pi\gamma}}{m_\pi^2} \frac{\mathcal{F}_{\pi NN}(q_\pi^2) \mathcal{F}_{a_2\pi\gamma}(q_\pi^2)}{q_\pi^2 - m_\pi^2} \bar{u}(p_4) \\ &\quad \times \gamma_5 \epsilon_{\mu\nu\alpha\beta} p_3^\mu T^{\nu\sigma}(p_3) p_1^\alpha e^\beta(p_1) (q_\pi)_\sigma u(p_2) \end{aligned} \quad (15)$$

for Fig. 1(a), and

$$\begin{aligned} \mathcal{M}_b &= \sqrt{2} \frac{g_{\pi NN} g_{a_2\pi\rho}}{m_\pi^2} \frac{e}{f_\rho} \frac{\mathcal{F}_{\pi NN}(q_\pi^2) \mathcal{F}_{a_2\pi\rho}(q_\pi^2)}{q_\pi^2 - m_\pi^2} \bar{u}(p_4) \\ &\quad \times \gamma_5 \epsilon_{\mu\nu\alpha\beta} p_3^\mu T^{\nu\sigma}(p_3) p_1^\alpha e^\beta(p_1) (q_\pi)_\sigma u(p_2) \end{aligned} \quad (16)$$

for Fig. 1(b). Here $e^\beta(p_1)$ and $T^{\nu\sigma}(p_3)$ are the photon polarization vector and the polarization vector of the a_2 , respectively, and $u(p_2)$ and $\bar{u}(p_4)$ are the Dirac spinors for the initial proton and the final neutron, respectively.

To describe the behavior at high photon energy, we introduce the Regge trajectories [18,31,47,48]

$$\frac{1}{q_\pi^2 - m_\pi^2} \rightarrow \mathcal{D}_\pi = \left(\frac{s}{s_{\text{scale}}} \right)^{\alpha_\pi(t)} \frac{\pi \alpha'_\pi e^{-i\pi\alpha_\pi(t)}}{\Gamma[1 + \alpha_\pi(t)] \sin[\pi\alpha_\pi(t)]}, \quad (17)$$

where α'_K is the slope of the trajectory and the scale factor s_{scale} is fixed at 1 GeV^2 , while $s = (p_1 + p_2)^2$ and $t = (p_2 - p_4)^2$ are the Mandelstam variables. In addition, the kaonic Regge trajectory $\alpha_K(t)$ is [18,31,47,48]

$$\alpha_\pi(t) = 0.7(t - m_\pi^2). \quad (18)$$

With $s = (p_1 + p_2)^2$, the unpolarized differential cross section for the $\gamma(p_1)p(p_2) \rightarrow a_2^+(p_3)n(p_4)$ process at the center of mass (c.m.) frame is given by

$$\frac{d\sigma}{d\cos\theta} = \frac{1}{32\pi s} \frac{|\vec{p}_3^{\text{c.m.}}|}{|\vec{p}_1^{\text{c.m.}}|} \left(\frac{1}{4} \sum_{\text{spins}} |\mathcal{M}_{a/b}|^2 \right), \quad (19)$$

where θ denotes the angle of the outgoing a_2^+ meson relative to the beam direction in the c.m. frame, while $\vec{p}_1^{\text{c.m.}}$ and $\vec{p}_3^{\text{c.m.}}$ are the three-momenta of the initial photon beam and the final a_2^+ , respectively.

III. RESULTS AND DISCUSSION

A. Cross section for the $\gamma p \rightarrow a_2^+ n$ reaction

Energy dependence of the cross section calculated above for each of the models for the fixed parameter $\Lambda_t = 1 \text{ GeV}$ of the monopole form factor is shown in Fig. 2. One can see that the difference between the models is about an order of magnitude. Fine-tuning of the parameter Λ_t can be performed on the basis of the experimental results.

The existing experimental data [23,49–52] for a_2 photoproduction at low energies are summarized in Table I and Fig. 3. The original data from [52] have been reanalyzed in [23] to take into account the actual branching ratio for the $a_2 \rightarrow 3\pi$ decay channel, since it was taken to be 100%. To fix the same problem we scale the result for the cross section and the error presented in [50] by the factor of 1.5. We also skip the result for $E_\gamma = 19.5 \text{ GeV}$, which seems to be in tension with the shape of the expected theoretical curves. The MINUIT code of the CERNLIB library was used to perform one-parameter χ^2 fits of the theoretical curves to the $\sigma_{\gamma p \rightarrow a_2^+ n}$ data. The free parameters involved and their fitted values are listed in Table II.

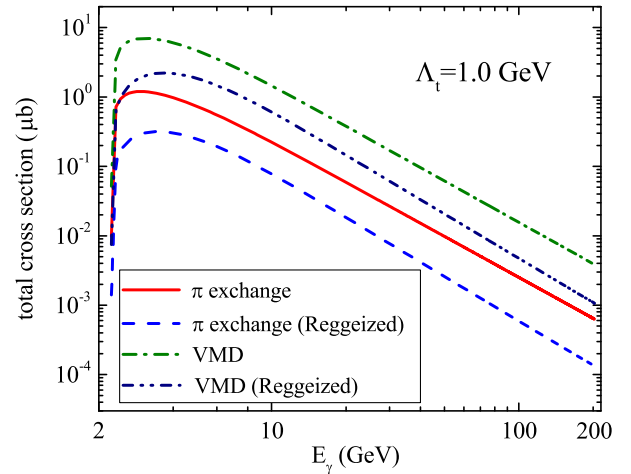


FIG. 2. Total cross section for the $\gamma p \rightarrow a_2^+ n$ reaction for the fixed parameter $\Lambda_t = 1 \text{ GeV}$.

TABLE I. The experimental data for a_2 photoproduction cross section. Here the beam energy E_γ is in the units of GeV, while the cross section $\sigma_{\gamma p \rightarrow a_2^+ n}$ is the units of μb .

E_γ	$\sigma_{\gamma p \rightarrow a_2^+ n}$	Data source
3.625 (3.25–4.0)	0.7 ± 0.3	[49]
4.2 (3.7–4.7)	1.2 ± 0.45	[50]
4.8 (4.3–5.25)	2.6 ± 0.6	[23,52]
5.1 (4.8–5.4)	0.81 ± 0.25	[51]
5.15 (4.0–6.3)	0.3 ± 0.3	[49]
5.25 (4.7–5.8)	0.9 ± 0.45	[50]
7.5 (6.8–8.2)	0.45 ± 0.45	[50]
19.5	0.29 ± 0.06	[23]

The fitted parameter Λ_t satisfies the expectation with a reasonable χ^2/ndf . And yet, it is found that the cases with Reggeized treatment need a larger Λ_t . For comparison, we also calculate the result with a dipole or exponential form factor. The fitted parameters Λ_d and R are listed in Tables III and IV, respectively. Figure 3 shows the fitted results with the three types of form factor. It is found that the difference is small in the result of improvements in three types of form factor. Therefore, in the following calculation, we only consider the case of the monopole form factor.

From Fig. 3(a) one can see that the experimental data (except the point at $E_\gamma = 4.8$ and 19.5 GeV) [23,49–52] for the total cross section of the $\gamma p \rightarrow a_2^+ n$ reaction are well reproduced with a small value of χ^2/ndf . The shape of the total cross section via π exchange is different from that of the VMD mechanism.

With the above equations and the fitted parameters as listed in Table II, the relevant physical results are calculated, as shown in Figs. 4–6.

In Fig. 4 we also present the variation of the total cross section of the $\gamma p \rightarrow a_2^+ n$ reaction within the typical uncertainties of the Λ_t values. From Fig. 4(a) it is seen that the total cross section via π exchange is more sensitive than that of the VMD mechanism to the values of Λ_t . Moreover, a comparison of the results from Figs. 4(a) and 4(b) reveals that the total cross section becomes less sensitive to the Λ_t values when the Reggeized treatment is added to the process of $\gamma p \rightarrow a_2^+ n$.

In Fig. 5, we show the differential cross section of $\gamma p \rightarrow a_2^+ n$ as a function of $-t$. It is obvious that there is a significant peak structure in the region of low $-t$, which increases rapidly near the threshold and then decreases slowly with increasing $-t$. However, it is seen that the shapes of the differential cross section $d\sigma/dt$ with the Reggeized treatment are much different from that without the Reggeized treatment at higher $-t$. The Reggeized treatment can lead to the differential cross section $d\sigma/dt$ decreasing rapidly with increasing $-t$, especially at higher energies.

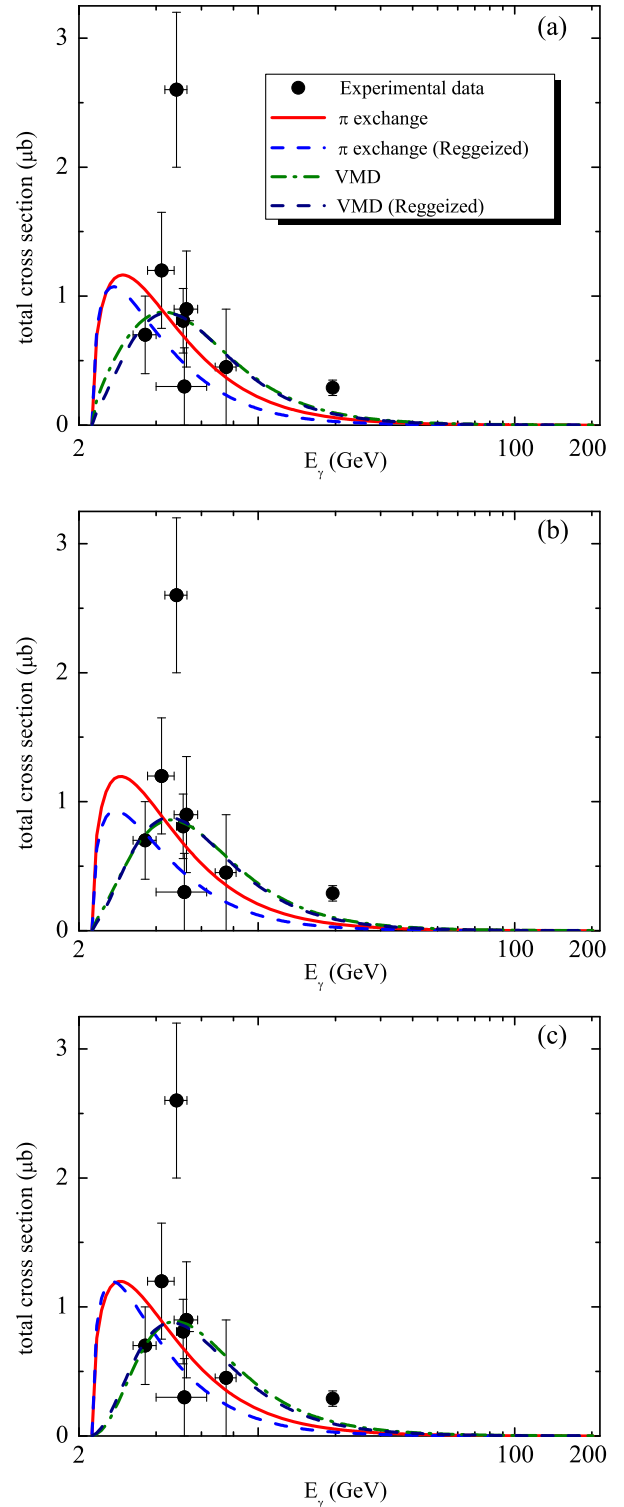


FIG. 3. Total cross section for the $\gamma p \rightarrow a_2^+ n$ reaction. The data are from [23,49–52]. Here, (a) is the result with the monopole form factor, while (b) and (c) are the results related to the dipole and exponential form factors correspondingly.

Figure 6 presents the differential cross section for the $\gamma p \rightarrow a_2^+ n$ reaction with or without the Reggeized treatment at different energies. It is seen that the differential

TABLE II. The fitted values of the free parameter Λ_t of the monopole form factor, while the cutoff Λ_t is in the units of GeV.

Type	Λ_t	χ^2/ndf
π exchange	0.99 ± 0.07	2.23
π exchange (Reggeized)	3.58 ± 0.66	2.73
VMD	0.35 ± 0.02	2.05
VMD (Reggeized)	0.46 ± 0.04	2.04

 TABLE III. The fitted values of the free parameter Λ_d of the dipole form factor, while the cutoff Λ_d is in the units of GeV.

Type	Λ_d	χ^2/ndf
π exchange	1.53 ± 0.11	2.26
π exchange (Reggeized)	3.79 ± 0.78	2.91
VMD	0.54 ± 0.03	2.07
VMD (Reggeized)	0.69 ± 0.06	2.05

 TABLE IV. The fitted values of the free parameter R of the exponential form factor, while R is in the units of GeV^{-1} .

Type	R	χ^2/ndf
π exchange	0.47 ± 0.03	2.26
π exchange (Reggeized)	0.10 ± 0.02	2.66
VMD	1.30 ± 0.07	2.10
VMD (Reggeized)	1.06 ± 0.09	2.06

cross section with the Reggeized treatment is very sensitive to the angle θ and makes a considerable contribution at forward angles.

B. Dalitz process $\gamma p \rightarrow \rho\pi n$

Considering the a_2 are usually detected in experiment via the $\rho\pi$ invariant mass, it would be useful to give the theoretical predictions of the differential cross section $d\sigma_{\gamma p \rightarrow a_2^+ n \rightarrow \rho\pi n}/dM_{\rho\pi}$ as a function of the beam energy E_γ , which could be tested by further experiment. Since the full decay width of the $a_2(1320)$ is small enough in comparison to its mass, the invariant mass distribution for the Dalitz process $\gamma p \rightarrow \rho\pi n$ can be defined with the two-body process [53]

$$\frac{d\sigma_{\gamma p \rightarrow \rho\pi n}}{dM_{\rho\pi}} \approx \frac{2m_{a_2} M_{\rho\pi}}{\pi} \frac{\sigma_{\gamma p \rightarrow a_2^+ n} \Gamma_{a_2 \rightarrow \rho\pi}}{(M_{\rho\pi}^2 - m_{a_2}^2)^2 + m_{a_2}^2 \Gamma_{a_2}^2},$$

where the full width $\Gamma_{a_2} = 107$ MeV and the partial width $\Gamma_{a_2 \rightarrow \rho\pi} = 75$ MeV are taken [42].

With the above equations and the fitted parameters as listed in Table II, the invariant-mass distribution $d\sigma_{\gamma p \rightarrow a_2^+ n \rightarrow \rho\pi n}/dM_{\rho\pi}$ for $E_\gamma = 3\text{--}200$ GeV is calculated,

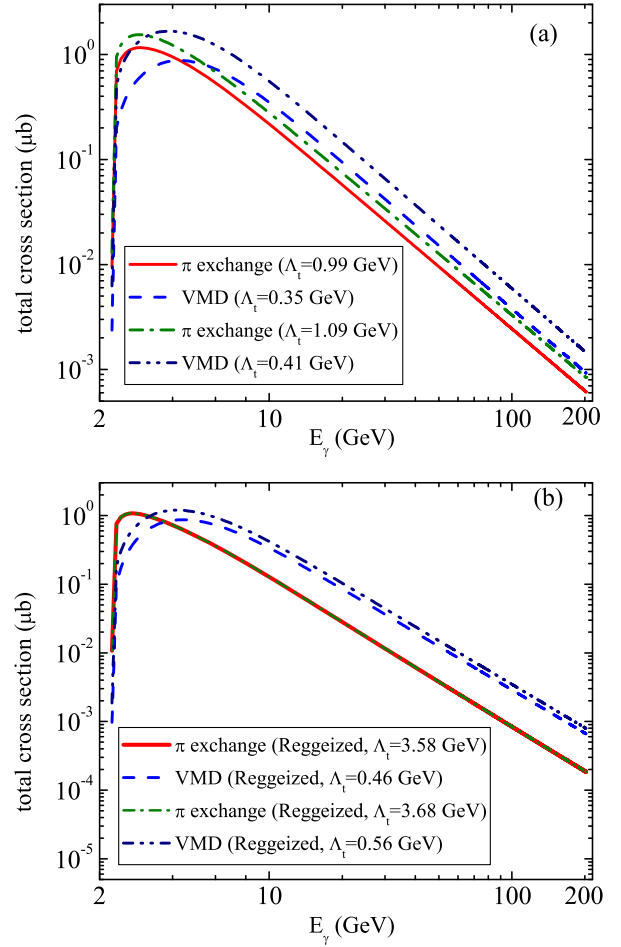


FIG. 4. (a) The total cross section of the $\gamma p \rightarrow a_2^+ n$ reaction for the different values of cutoff parameter Λ_t . (b) Same as in (a), but for the case of the Regge trajectory exchange.

as shown in Fig. 7. It is seen that there exists an obvious peak at $M_{\rho\pi} \approx 1.32$ GeV.

IV. POSSIBILITY OF THE EXPERIMENTAL TEST AT COMPASS

The COMPASS experiment [54] is situated at the M2 beam line of the CERN Super Proton Synchrotron. Since 2002 it has obtained experimental data for positive muons scattering of 160 GeV/c (2002–2010) or 200 GeV/c momentum (2011) off solid ${}^6\text{LiD}$ (2002–2004) or NH_3 polarized targets (2006–2011). Particle tracking and identification is performed in a two-stage spectrometer covering a wide kinematical range. The trigger system comprises hodoscope counters and hadron calorimeters.

According to the presented calculations of the a_2 production cross section and previously published COMPASS results for exclusive photoproduction of ρ^0 [55] and J/ψ [56], we can conclude that thousands of a_2^\pm mesons could be produced per year of data taking via the exclusive charge-exchange reactions $\gamma^* p \rightarrow a_2^\pm n$ and

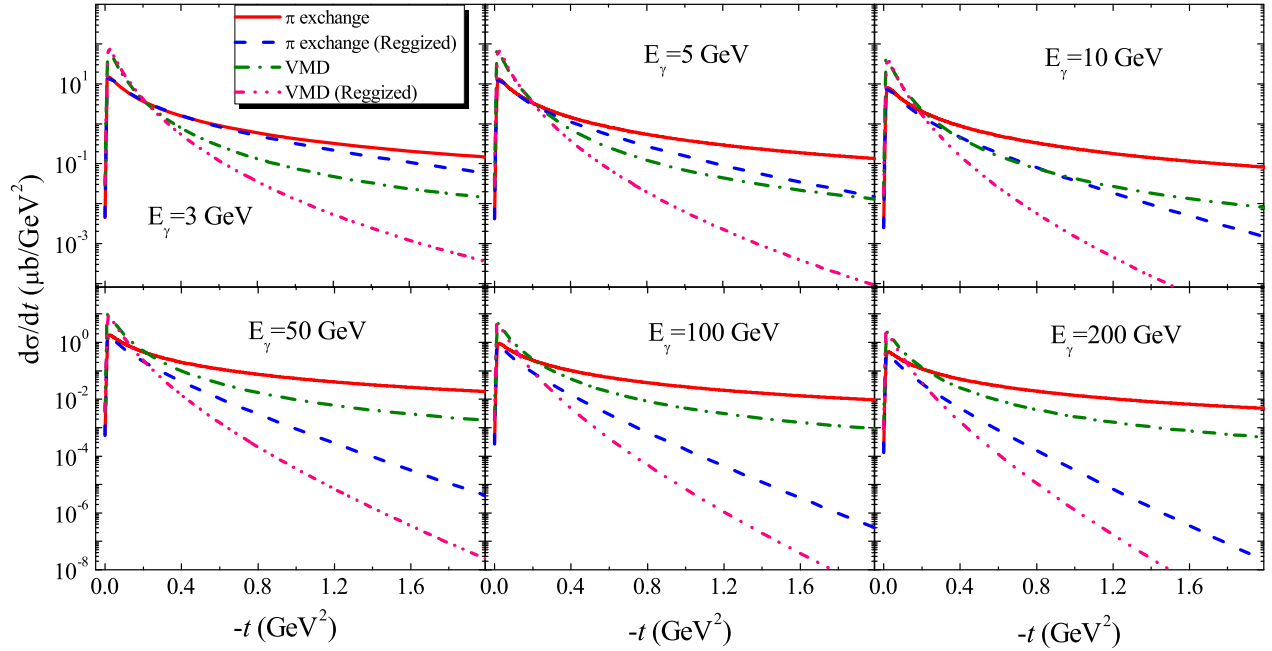


FIG. 5. The differential cross section of $\gamma p \rightarrow a_2^+ n$ as a function of $-t$ at $E_\gamma = 3\text{--}200$ GeV.

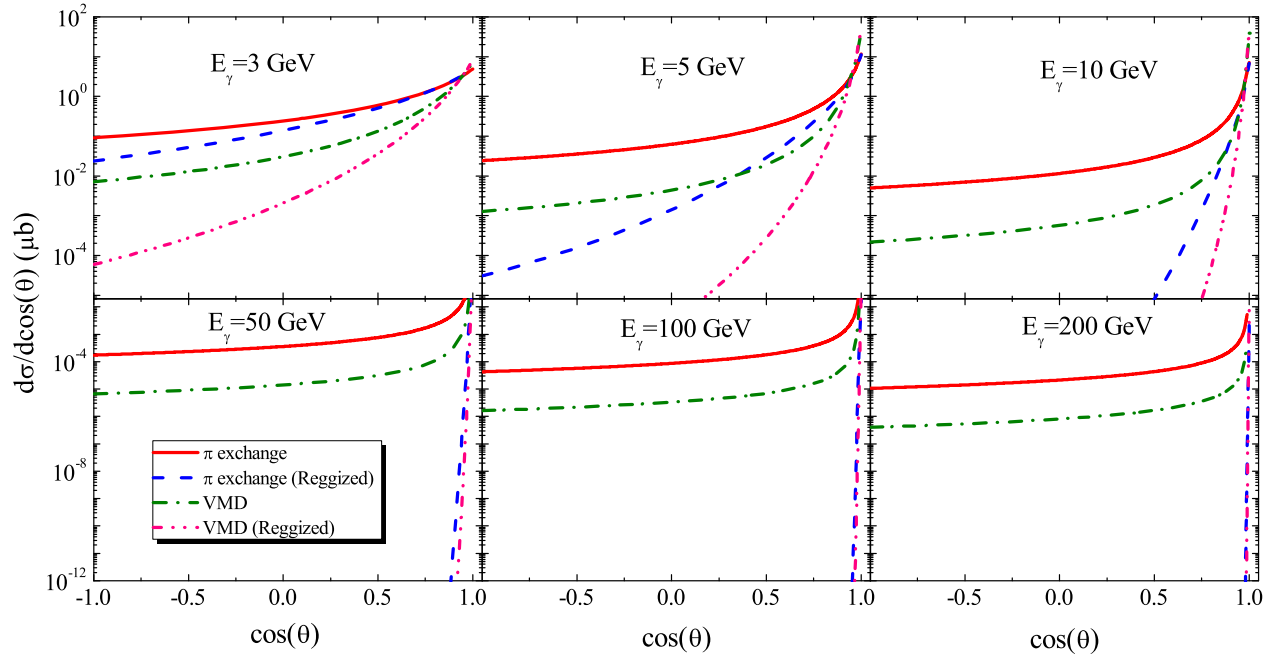


FIG. 6. The differential cross section $d\sigma/d\cos\theta$ for the $a_2(1320)$ photoproduction from the proton as a function of $\cos\theta$ at $E_\gamma = 3\text{--}200$ GeV.

$\gamma^* n \rightarrow a_2^- p$ (but the recoil nucleon cannot be detected). The energy of a virtual photon covers the range from about 20 GeV and up to 180 GeV. The obtained data can be used to clarify the mechanism of the a_2 production and the role of the Reggeized treatment at high energies. Nevertheless, most of the a_2^\pm mesons at such energies are produced nonexclusively via the Pomeron exchange mechanism.

Such events could produce a strong background under poor exclusivity control. Additional systematics could come from the process $\gamma^* p \rightarrow a_2^- \Delta^{++}$ (the cross section of this reaction is of the same order of magnitude [57]) because the COMPASS setup is not able to reconstruct a decay of low-energy Δ^{++} in a regular way. Nuclear effects in a_2 photoproduction off the lithium-6, deuterium, and

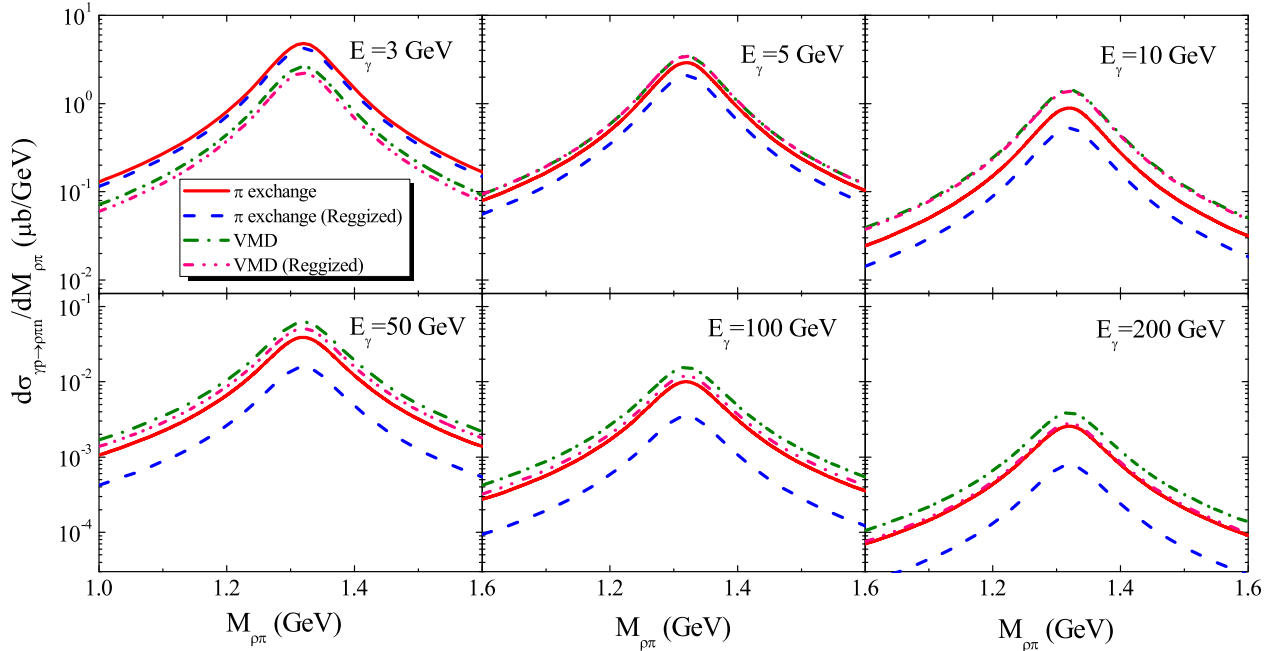


FIG. 7. Differential cross section $d\sigma_{\gamma p \rightarrow a_2^+ n} / dM_{\rho\pi}$ as a function of $M_{\rho\pi}$ at $E_\gamma = 3\text{--}200$ GeV.

nitrogen nuclei should also be taken into account in an appropriate way.

The forthcoming upgrade of the COMPASS setup related to the planned data taking within the framework of the GPD program [58] could provide better conditions for experimental study of the reaction $\gamma^* p \rightarrow a_2^+ n$ and partially eliminate problems mentioned above. The new 2.5 m long liquid hydrogen target surrounded by a 4 m long recoil proton detector will be used. The absence of the neutrons in the target will remove one exclusive production channel for a_2^- . The recoil proton detector serves the double purpose: to reconstruct and identify recoil protons via time-of-flight and energy loss measurements. Since the reaction $\gamma^* p \rightarrow a_2^+ n$ does not have a recoil proton in the final state, any activity in the recoil proton detector could be used as the veto in the off-line analysis. In addition, the recoil proton detector will be able to detect the $\Delta^{++} \rightarrow p\pi^+$ decay. A significant impact on the exclusivity control efficiency will be made by the planned upgrade of the electromagnetic calorimetry system.

V. SUMMARY

Within the framework of the effective Lagrangian approach and Regge model, the $a_2(1320)$ photoproduction from the proton is investigated.

The obtained numerical results indicate the following:

- (I) The total cross section $\gamma p \rightarrow a_2^+ n$ related to the experimental data [23,49–52] is well reproduced with a reasonable value of χ^2/ndf . Although the monopole form factor was used in the calculations,

the dipole and exponential form factors were also tested. It is found that the total cross section becomes less sensitive to the Λ_t values when the Reggeized treatment is added.

- (II) The shapes of the differential cross section $d\sigma/dt$ with the Reggeized treatment are much different from that without the Reggeized treatment at higher $-t$. The Reggeized treatment can lead to the differential cross section $d\sigma/dt$ decreasing rapidly with the increasing $-t$, especially at higher energies.
- (III) The differential cross section $d\sigma/d\cos\theta$ with the Reggeized treatment is very sensitive to the angle θ and makes a considerable contribution at forward angles.
- (IV) The invariant mass distribution for the Dalitz process $\gamma p \rightarrow \rho\pi n$ shows an obvious peak at $M_{\rho\pi} \approx 1.32$ GeV, which can be checked by further experiment.
- (V) For comparison, it is found that the cross section of the $\gamma n \rightarrow a_2^- p$ process is almost the same as that of the $\gamma p \rightarrow a_2^+ n$ reaction. Thus, the above theoretical results are valid to the $\gamma n \rightarrow a_2^- p$ channel.

To sum up, we suggest testing our prediction for the cross section of the $\gamma p \rightarrow a_2^+ n$ process at the COMPASS facility at CERN. Such a test could provide important information for clarifying the production mechanism of the $a_2(1320)$ and the role of the Reggeized treatment at high energies. Nevertheless, the precise measurements near the threshold, where the difference between the predictions of the production models is maximal, are also important.

ACKNOWLEDGMENTS

X. Y. W. is grateful to Helmut Haberzettl and Jun He for useful discussions about Regge theory.

-
- [1] M. Nielsen, F. S. Navarra, and S. H. Lee, *Phys. Rep.* **497**, 41 (2010).
- [2] X. Liu, *Chin. Sci. Bull.* **59**, 3815 (2014).
- [3] R. Aaij *et al.* (LHCb Collaboration), *Phys. Rev. Lett.* **112**, 222002 (2014).
- [4] R. Aaij *et al.* (LHCb Collaboration), *Phys. Rev. Lett.* **115**, 072001 (2015).
- [5] X.-H. Liu, Q. Zhao, and F. E. Close, *Phys. Rev. D* **77**, 094005 (2008).
- [6] J. He and X. Liu, *Phys. Rev. D* **80**, 114007 (2009).
- [7] Q.-Y. Lin, X. Liu, and H.-S. Xu, *Phys. Rev. D* **89**, 034016 (2014).
- [8] Q. Wang, X.-H. Liu, and Q. Zhao, *Phys. Rev. D* **92**, 034022 (2015).
- [9] M. Karliner and J. Rosner, *Phys. Lett. B* **752**, 329 (2016).
- [10] P. D. B. Collins, *An Introduction to Regge Theory and High Energy Physics* (Cambridge University Press, Cambridge, UK, 1977).
- [11] V. Gribov, *Strong Interactions of Hadrons at High Energies* (Cambridge University Press, Cambridge, UK, 2009).
- [12] W.-T. Chiang, S. N. Yang, L. Tiator, M. Vanderhaeghen, and D. Drechsel, *Phys. Rev. C* **68**, 045202 (2003).
- [13] T. Regge, *Nuovo Cimento* **14**, 951 (1959).
- [14] T. Regge, *Nuovo Cimento* **18**, 947 (1960).
- [15] R. J. Eden, *Rep. Prog. Phys.* **34**, 995 (1971).
- [16] T. Corthals, J. Ryckebusch, and T. Van Cauteren, *Phys. Rev. C* **73**, 045207 (2006).
- [17] J. K. Storrow, *Rep. Prog. Phys.* **50**, 1229 (1987).
- [18] M. Guidal, J. M. Laget, and M. Vanderhaeghen, *Nucl. Phys. A* **627**, 645 (1997).
- [19] G. Galatà, *Phys. Rev. C* **83**, 065203 (2011).
- [20] J. He, *Phys. Rev. C* **89**, 055204 (2014).
- [21] E. Wang, Ju-Jun Xie, and J. Nieves, *Phys. Rev. C* **90**, 065203 (2014).
- [22] H. Högaasen, J. Högaasen, R. Keyser, and B. E. Y. Svensson, *Nuovo Cimento A* **42**, 323 (1966).
- [23] G. T. Condo, *Phys. Rev. D* **48**, 3045 (1993).
- [24] D. Morrison, *Phys. Lett.* **22**, 528 (1966).
- [25] A. P. Szczepaniak and M. Swat, *Phys. Lett. B* **516**, 72 (2001).
- [26] T. Bauer and D. R. Yennie, *Phys. Lett.* **60B**, 165 (1976).
- [27] T. Bauer and D. R. Yennie, *Phys. Lett.* **60B**, 169 (1976).
- [28] T. H. Bauer, R. D. Spital, D. R. Yennie, and F. M. Pipkin, *Rev. Mod. Phys.* **50**, 261 (1978); **51**, 407(E) (1979).
- [29] B. S. Zou and F. Hussain, *Phys. Rev. C* **67**, 015204 (2003).
- [30] X. Y. Wang, J. J. Xie, and X. R. Chen, *Phys. Rev. D* **91**, 014032 (2015).
- [31] X. Y. Wang, X. R. Chen, and A. Guskov, *Phys. Rev. D* **92**, 094017 (2015).
- [32] X. Y. Wang and X. R. Chen, *Europhys. Lett.* **109**, 41001 (2015).
- [33] X. Y. Wang and X. R. Chen, *Eur. Phys. J. A* **51**, 85 (2015).
- [34] X. Y. Wang, A. Guskov, and X. R. Chen, *Phys. Rev. D* **92**, 094032 (2015).
- [35] K. Tsushima, A. Sibirtsev, A. W. Thomas, and G. Q. Li, *Phys. Rev. C* **59**, 369 (1999); **61**, 029903(E) (2000).
- [36] Z. Lin, C. M. Ko, and B. Zhang, *Phys. Rev. C* **61**, 024904 (2000).
- [37] V. Baru, C. Hanhart, M. Hoferichter, B. Kubis, A. Nogga, and D. R. Phillips, *Nucl. Phys. A* **872**, 69 (2011).
- [38] N. Levy, P. Singer, and S. Toaff, *Phys. Rev. D* **13**, 2662 (1976).
- [39] J. Babcock and J. L. Rosner, *Phys. Rev. D* **14**, 1286 (1976).
- [40] K. Bongardt, W. Gamp, and H. Genz, *Z. Phys. C* **3**, 233 (1980).
- [41] Z. E. S. Uy, *Phys. Rev. D* **29**, 574 (1984).
- [42] K. A. Olive *et al.* (Particle Data Group), *Chin. Phys. C* **38**, 090001 (2014).
- [43] T. Feuster and U. Mosel, *Phys. Rev. C* **58**, 457 (1998).
- [44] T. Feuster and U. Mosel, *Phys. Rev. C* **59**, 460 (1999).
- [45] V. P. Goncalves, F. S. Navarra, and D. Spiering, arXiv: 1510.01512.
- [46] F. Carvalho, V. P. Goncalves, D. Spiering, and F. S. Navarra, *Phys. Lett. B* **752**, 76 (2016).
- [47] A. I. Titov, B. Kämpfer, S. Daté, and Y. Ohashi, *Phys. Rev. C* **72**, 035206 (2005); **72**, 049901(E) (2005).
- [48] T. Corthals, T. Van Cauteren, J. Ryckebusch, and D. G. Ireland, *Phys. Rev. C* **75**, 045204 (2007).
- [49] W. Struczinski *et al.* (Aachen-Hamburg-Heidelberg-Munich Collaboration), *Nucl. Phys. B* **108**, 45 (1976).
- [50] Y. Eisenberg *et al.*, *Phys. Rev. D* **5**, 15 (1972).
- [51] M. Nozar *et al.* (CLAS Collaboration), *Phys. Rev. Lett.* **102**, 102002 (2009).
- [52] Y. Eisenberg *et al.*, *Phys. Rev. Lett.* **23**, 1322 (1969).
- [53] S. I. Nam and H. K. Jo, arXiv:1503.00419.
- [54] P. Abbon *et al.* (COMPASS Collaboration), *Nucl. Instrum. Methods Phys. Res., Sect. A* **577**, 455 (2007).
- [55] C. Adolph *et al.*, *Phys. Lett. B* **731**, 19 (2014).
- [56] C. Adolph *et al.* (COMPASS Collaboration), *Phys. Lett. B* **742**, 330 (2015).
- [57] G. T. Condo *et al.*, *Phys. Rev. D* **41**, 3317 (1990).
- [58] M. Alekseev (COMPASS Collaboration), Report No. SPSC-2010-014/P-340.